Proceedings of the 2010 Joint Rail Conference
JRC2010
April 27-29, 2010, Urbana, Illinois, USA

JRC2010-36219

EVALUATING THE POTENTIAL FOR DAMAGING HYDRAULIC PRESSURE IN THE CONCRETE TIE RAIL SEAT

John C. Zeman
Univ. of Illinois at Urbana-Champaign
Dept. of Civil and Environ. Engineering
205 N Mathews Ave,
Urbana, IL 61801
jzeman2@gmail.com

J. Riley Edwards
Univ. of Illinois at Urbana-Champaign
Dept. of Civil and Environ. Engineering
205 N Mathews Ave,
Urbana, IL 61801
(217) 244-7417
jedward2@illinois.edu

David A. Lange
Univ. of Illinois at Urbana-Champaign
Dept. of Civil and Environ. Engineering
205 N Mathews Ave,
Urbana, IL 61801
dlange@illinois.edu

Christopher P.L. Barkan
Univ. of Illinois at Urbana-Champaign
Dept. of Civil and Environ. Engineering
205 N Mathews Ave,
Urbana, IL 61801
cbarkan@illinois.edu

ABSTRACT

Rail seat deterioration (RSD) is the most critical problem with concrete tie performance on North American freight railroads. Currently, the problem is not sufficiently understood to allow for effective solutions. RSD is considered to have up to five potential mechanisms, and this paper investigates one of them: hydraulic pressure cracking. A model of the effective stress in a concrete tie rail seat – considering the contributions of a uniform vertical load, a uniform lateral load, a prestressed beam on an elastic foundation, and pore pressure to the state of stress – was created to determine what surface water pressures at the rail seat could lead to damaging pore water pressures in the concrete. A laboratory test setup and procedure were devised to measure the surface water pressure in a laboratory rail seat using tie pads of differing material composition and geometry. Results show that the magnitude of the pressure generated and the rate of pressure dissipation with many load cycles depends on the pad material and surface geometry. Comparing the effective stress model and the measured surface pressures, hydraulic pressure cracking appears to be a feasible mechanism for RSD given the correct combination of dynamic rail seat loads, sufficient moisture, and a tie pad surface that develops high pressure.

INTRODUCTION

Rail seat deterioration (RSD) is concrete deterioration underneath the rail on a concrete railroad tie. This deterioration leads to track geometry defects such as wide gauge and allows for accelerated deterioration of the rail-to-tie fastening system. RSD is difficult to detect without removing the rail and fastening system and examining the concrete rail seat. Maintenance measures currently used to combat RSD are regular replacement of the tie pad, periodic replacement of the fastening components, restoration of the proper rail seat surface with an epoxy or polyurethane, or removal of the whole tie from service [1, 2]. A survey of freight railroads in the US and Canada conducted by the University of Illinois at Urbana-Champaign concluded that RSD was the most critical problem with concrete ties on their routes [3]. Prestressed concrete ties have the potential to withstand a combination of heavy axle loads and high tonnage that other tie materials

cannot. Also, ballasted concrete-tie track or slab track are the preferred method of track support for high-speed operations due to their stiff support and tighter geometric tolerances [1, 2]. For these reasons, improving the performance of concrete ties will be very beneficial to the railroad industry.

Learning how to effectively eliminate or mitigate RSD will reduce the risk of concrete ties failing prematurely or requiring excessive maintenance. This would lower the life-cycle costs and help make concrete ties a more viable economic alternative to timber ties in North America. The US and Canadian railroads have learned much about RSD since it was first identified in the mid-1980's [4], such as the importance of wheel loads, moisture, abrasive fines, and tightness of the fastening system to the problem's development [1, 2]. There are multiple possible mechanisms for RSD, but the concrete deterioration process is not wholly understood. Currently, there is evidence that abrasion, freeze-thaw cracking, crushing, or hydraulic pressure cracking may contribute to RSD [4, 5]. Little evidence has been found to suggest that alkali-silica reactivity (ASR) or cavitation erosion is contributing to RSD [4]. This research study is an effort to understand the mechanics of the concrete deterioration in RSD by focusing on moisture-driven mechanisms, such as hydraulic pressure cracking. By understanding which deterioration mechanisms are acting on the concrete, it will be possible to develop more effective methods to solve or mitigate RSD.

The theory on hydraulic pressure cracking claims that pore pressures in the concrete become large enough that the concrete's tensile strength is exceeded, resulting in cracking or spalling [4]. In order to evaluate the feasibility of this theory, two elements were examined: (1) the specific pore pressure required to damage the concrete, and (2) the expected pore pressure in a typical concrete railroad tie.

EFFECTIVE STRESS MODEL

To estimate the pore pressure required to do damage to the concrete, a model was created to calculate the effective stress beneath the center of the rail seat. This model is an adaptation of an approach developed by Bakharev [4]. The effective stress of the concrete is the total stress – the sum of all the mechanical stresses acting on an element of concrete – minus the pore pressure. With this formulation, stress is taken as positive when it is compressive, and the pore pressure exerts a tensile stress on the concrete, similar to what is experienced by the walls of a pressure vessel. It is the effective stress that must be compared with the concrete's strength to determine if damage will occur.

Bakharev's effective stress model was for two-dimensional stresses, considering only the vertical wheel load's contribution to total stress. Our model also incorporates the contributions of lateral loads, prestress, and flexure in three dimensions. We directly use Bakharev's formula for pore pressure distribution, expanded to three dimensions.

Considering the effective stress in a concrete tie in three dimensions, the total stress state was taken as the sum of the stress states from a uniform vertical load, a uniform horizontal load, and a prestressed beam on an elastic foundation. Then the total stress state was converted to a principal stress state that can be expressed by three mutually perpendicular normal stresses and no shear stress [6]. The minimum of these three stresses is referred to as the minor principal stress, and it represents the direction in which the concrete is most susceptible to damage from pore pressure. The minor principal stress is the total stress term used in the effective stress equation.

Total Stress

For the uniform vertical load (normal to the rail seat), Holl's equations were used to find the total stress beneath the center of a square 42 square-inch (0.027 square-meter) rail seat, assuming an elastic stress distribution with Poisson's ratio of 0.5 [7]. The Poisson's ratio of concrete is typically around 0.2 [8]. This discrepancy between the model and the actual concrete material was accepted because the resulting equations for a three-dimensional state of stress were readily available. For elastic stress distributions, choosing a larger Poisson's ratio generally results in a stiffer material, thus greater confining stresses than would be observed with a smaller Poisson's ratio [7]. The normal load on the rail seat was estimated as approximately 50% of a rail car wheel load, accounting for load distribution among adjacent ties and the cant of the rail [1, 2]. Because Holl's equations directly apply to one fourth of the loaded area, they were multiplied by four to apply superposition:

$$S_V = 4\begin{bmatrix} \{\sigma_x\}_V & \{\tau_{xy}\}_V & \{\tau_{xz}\}_V \\ \{\tau_{xy}\}_V & \{\sigma_y\}_V & \{\tau_{yz}\}_V \\ \{\tau_{xz}\}_V & \{\tau_{yz}\}_V & \{\sigma_z\}_V \end{bmatrix} \quad (1)$$

Similar to the calculation of total stress from a uniform vertical load, the total stress from a uniform horizontal load was calculated using equations from Holl – again assuming a Poisson's ratio of 0.5. The lateral load on the rail seat was estimated as 52% of the normal load – effectively using a lateral-to-vertical load ratio (L/V) of 0.52 [1, 2]. Holl's coordinates were such that the horizontal load was in the positive x-direction, but our coordinates have the horizontal load in the negative y-direction [7]. To correct for the differing coordinates, Holl's state of stress was transformed (rotated 90-degrees) to our coordinate system before entering the effective stress model. The transformed total stress state, referencing the equations from Holl's coordinates, is:

$$S_H = 4\begin{bmatrix} \{\sigma_y\}_H & -\{\tau_{xy}\}_H & \{\tau_{yz}\}_H \\ -\{\tau_{xy}\}_H & \{\sigma_x\}_H & -\{\tau_{xz}\}_H \\ \{\tau_{yz}\}_H & -\{\tau_{xz}\}_H & \{\sigma_z\}_H \end{bmatrix} \quad (2)$$

To consider the contributions of flexure and prestress, a model of a prestressed Timoshenko beam on an elastic foundation was developed. The components of the model are illustrated in Figure 1, with the variables defined in the Nomenclature section near the end of this article. A Timoshenko beam is a planar beam where the vertical deflection and in-plane rotation of the beam are considered independent variables. The bending moment and shear in the beam were determined by constitutive relationships with the deflection and rotation. Typically the axial strain is neglected, as was done here. The principal of virtual work was applied using the Galerkin method, which is a special form of the Ritz approximation, to estimate the deflection and rotation for many different scenarios [6].

The rail seat load was assumed to be uniformly distributed over the width of the base-of-rail (typically 6 inches, or 15.2 centimeters). The prestress at the ends of the tie is zero because of the open boundary. Over a certain development length, the prestress in the tendons builds up to its nominal value. This development was assumed to be 60 times the diameter of the tendons (wires or strands) [9]. The prestress in a real concrete tie is placed eccentrically relative to the neutral axis of the section to create the prestress bending moment, and the eccentricity changes as the section changes along the tie's length. For simplicity, however, this model of the tie was assumed to have a uniform rectangular cross-section, choosing an effective cross-sectional area and an effective moment of inertia along the length of the tie. In the absence of a changing section, the change in eccentricity was modeled to mimic what is common in many concrete ties currently in North America, as illustrated in Figure 1. Next, the prestress force was multiplied by the eccentricity at each point to get the applied prestress bending moment.

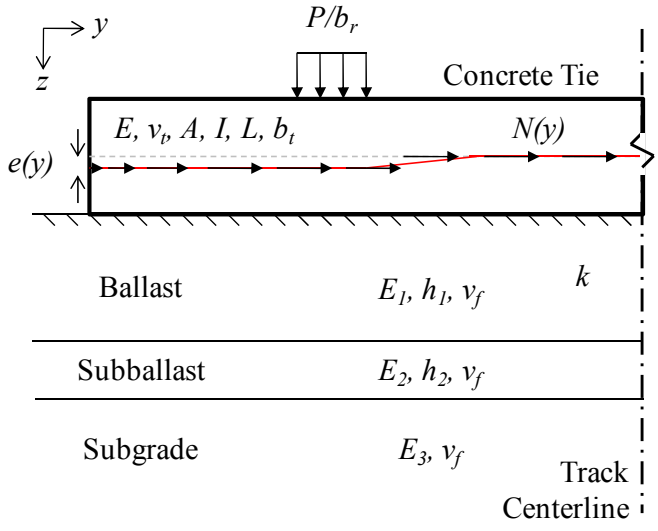

FIGURE 1. MODEL OF A PRESTRESSED BEAM ON AN ELASTIC FOUNDATION

The foundation reaction was represented by *kw(y)*. For estimating the foundation stiffness *k*, a range of values can bound the problem and provides a reasonable range of solutions [10]. There are many different approaches to estimating the foundation reaction from a granular material. The approach used here was adapted from Cai et al [11], selecting a different approach to estimate the foundation's effective resilient modulus, E_f:

$$k = \frac{0.65E_f}{(1-\nu_f)^2}\sqrt{\frac{E_f b_t^4}{EI}} \tag{3}$$

Odemark's method was selected for estimating E_f because it has been found to perform best when the relative stiffness of the foundation layers decreases with depth. Odemark's method assumes a Poisson's ratio of 0.5, which is generally not correct for ballast, subballast, and subgrade materials [7, 10].

Our model of a beam on an elastic foundation was partially verified by comparing its results without prestress and the results from Hetenyi's closed-form solution for an Euler-Bernoulli beam [12]. The deflection and in-plane rotations were nearly identical, and the differences between the shear and moment values were not great, with Hetenyi's equations yielding slightly larger values. The differences between Timoshenko and Euler-Bernoulli assumptions can probably account for the differences in our results. Additionally, Hetenyi used point loads at the rail seat, while we used distributed loads.

The shear force and bending moment from the beam model were converted to shear stress and normal stress at different depths, assuming constant (average) shear stress in the section and a linear flexural stress distribution:

$$\{\tau_{yz}\}_B = \frac{V}{A} \tag{4}$$

$$\{\sigma_y\}_B = \frac{M(c-z)}{I} + \frac{N}{A} \tag{5}$$

By assuming planar bending and an isotropic material, the stress components not on the face of a beam's cross-section are not affected by prestress or flexure [13]:

$$\mathrm{S}_B = \begin{bmatrix} 0 & 0 & 0 \\ 0 & \{\sigma_y\}_B & \{\tau_{yz}\}_B \\ 0 & \{\tau_{yz}\}_B & 0 \end{bmatrix} \tag{6}$$

The total stress state in the *xyz* coordinates was calculated as the superposition of (1), (2), and (6):

$$\mathrm{S}_{xyz} = \mathrm{S}_V + \mathrm{S}_H + \mathrm{S}_B \tag{7}$$

The principal directions and stresses were found by solving an eigenvalue problem with the state of total stress [6].

Pore Pressure

To estimate the pore pressure in the concrete for this study, the following approach was adapted from Bakharev's work on RSD. The pore water is assumed to obey Darcy's law flow. By assuming a fully saturated concrete, imposing conservation of mass flow, and noting that the permeability of concrete is nonzero, Bakharev showed that the pore pressure has to satisfy a Laplace differential equation [4]:

$$\frac{\partial^2 u}{\partial x^2}+\frac{\partial^2 u}{\partial y^2}+\frac{\partial^2 u}{\partial z^2}=0 \qquad (8)$$

The boundary conditions for this problem are that the pore pressure u is zero above the rail seat surface and that u at the surface is equal to p, a uniform surface pressure on the rail seat area.

Looking at the pore pressure below the center of the rail seat and assuming a square rail seat with sides b_r, Bakharev's solution to (8) simplifies to:

$$u=\frac{2p}{\pi}\left[\arctan\left(\frac{b_r}{2z}\right)\right] \qquad (9)$$

This equation can be used to estimate the pore pressure in a fully saturated concrete tie resulting from pressurized water at the rail seat surface. The general solution, not shown here, can be used to evaluate pore pressure away from the center of the rail seat.

Pascal's law states that a fluid exerts pressure equally on and normal to all surfaces of its container [14]. So in terms of a state of stress in any coordinate system, the pore pressure can be expressed as equal normal stresses without any shear [6].

Damage Limits

To estimate the strength and fatigue limits for concrete used in concrete ties, it was assumed that the tensile strength could represent the strength limit and approximately 50% of the tensile strength could represent the fatigue limit [8]:

$$\mathrm{S'=S-U}=\begin{bmatrix}\sigma_1-u & 0 & 0\\ 0 & \sigma_2-u & 0\\ 0 & 0 & \sigma_3-u\end{bmatrix}\leq\begin{matrix}\{f_t'\}_{Str}\\ or\\ \{\frac{1}{2}f_t'\}_{Fat}\end{matrix} \qquad (10)$$

The tensile strength was approximated as 10% of the 28-day compressive strength [8]. Because AREMA recommends a minimum compressive strength of 7,000 pounds per square inch (psi) or 48.3 megapascals (MPa) [15], we used 700 psi (4.83 MPa) as the tensile strength and 350 psi (2.41 MPa) as the fatigue limit. These limits are in terms of effective stress (tensile). By rearranging the effective stress equation and considering our pore pressure model, the limits were put in terms of surface pressure, as illustrated in Figure 2. See the Appendix for the conversions from US customary units to SI units.

The limits on surface pressure, p, were defined by finding the minimum pore pressure, u, curves that intersected the damage limits. As shown in Figure 2, the red curves corresponding to p = 720 psi gauge (psig) and p = 1180 psig (4.97 MPa and 8.14 MPa, respectively) are the minimum curves that intersect the fatigue limit and strength limit curves, respectively. The damage limits were defined by the effective stress at points around 1 to 2 inches (25 to 50 millimeters) below the rail seat surface in Figure 2 and for other magnitudes of load as well, due to the curvature of the damage limit curves. In her microscopy study of deteriorated rail seats, Bakharev found microcracks originating at approximately the same depth. She concluded that these microcracks could have been caused by either hydraulic pressure or freeze-thaw cycles [4].

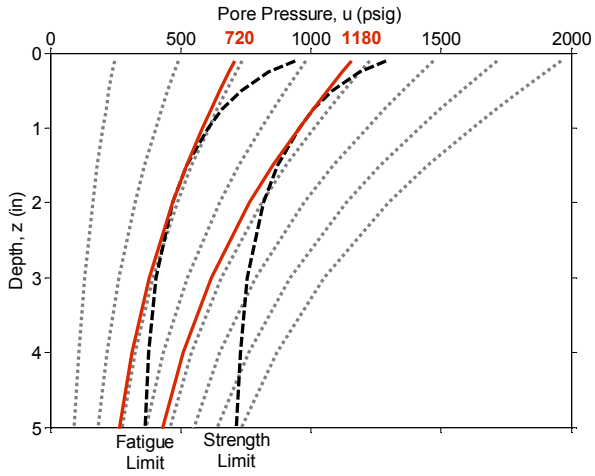

FIGURE 2. CONCRETE PORE PRESSURE AND DAMAGE LIMITS FOR 40-KIP APPLIED LOAD

By performing a sensitivity analysis on the effective stress model, it was determined that the uniform vertical load made the most significant contribution to the minor principal stress; therefore, it had the greatest impact on the damage limits. The uniform lateral load and prestressed beam contributions only affected the minor principal stress in the upper 2 inches (50 millimeters) of the tie, accounting for the curvature of the damage limits in Figure 2. Below approximately 2 inches (50 millimeters), the lateral load and prestress/flexure have little influence on the minor principal stress. This is because the minor principal stress was mostly oriented along the axis of the rail, in the x-direction. That is the direction of least total stress because the applied loads considered were only vertical, in the z-direction, or along the axis of the tie, in the y-direction.

LABORATORY TESTS

In previous work on hydraulic pressure cracking, it was assumed that the surface pressure p was equal to the uniform vertical load stress [4]. A laboratory setup and procedure were devised to measure p in a saturated, laboratory rail seat for different tie pads and loading scenarios to determine the validity of this assumption and whether the tie pad material or surface geometry affects the pressure generated.

Materials

In order to measure surface water pressure developed by simulated rail car loads on a mock concrete tie rail seat, a 6,000-psig-rated (41.4-MPa-rated) pressure transducer was placed in a concrete block and protected by a steel pipe which was cast in the specimen. The concrete had an average 28-day compressive strength of approximately 8,000 psi (55.2 MPa), and the block was capped with a sulfur compound to improve the block and base plate interface. The pressure transducer's orifice has an inner diameter of 0.6 inches (15 millimeters) and is 3.75 inches (95 millimeters) deep, and was placed flush with the block's "rail seat" surface.

A 100-kip (445-kilonewton (kN)) MTS servo-hydraulic actuator was used to apply normal loads to the tie pads on top of the instrumented concrete blocks. The concrete blocks were placed in a steel-based, plexiglass tank to hold water during the tests [1, 2].

Nine tie pads of different materials and surface geometries were considered in this study, including two types of pad assemblies. The tie pad surfaces that were tested were flat polyurethane, grooved polyurethane, dimpled polyurethane, flat ethyl-vinyl acetate (EVA), dimpled EVA, dimpled santoprene, a studded pad, a two-part assembly with a flat plastic bottom, and a three-part assembly with a flat foam bottom. Examples of the surface geometries are shown in Figure 3.

Procedure

After making some simplifying assumptions about a 286-kip (130-metric-ton) gross rail car load, the static normal force on one rail seat would be approximately 20 kips (89 kN), while the dynamic normal force on one rail seat could be as high as 60 kips (267 kN) or more [2, 15].

Over 180 unique scenarios were tested, and at least one replication was conducted per scenario. The tests involved cyclic loading of the concrete block, running the load from a minimum of 5 kips (22 kN) up to a maximum load, chosen from 20, 30, 40, 50, or 60 kips (89, 134, 178, 223, or 267 kN). The waveform of the load was chosen from trapezoidal wave (ramping at 200 kips (890 kN) per second), square wave, or sinusoidal wave (frequency of 2 or 4 Hertz (Hz)). The trapezoidal and square wave tests were run at 0.5 Hz frequency. The water level in the tank was varied from 0 to 6 inches (15 centimeters) above the rail seat surface, with 6 inches (15 centimeters) being the typical water level.

When running the tests, water was filled to the desired level, the pad under consideration was placed on the block, and the actuator was lowered to contact to secure the pad in place. When a pad with surface geometry was used, the dimensions of the pad and the block were used to align the pad indentations in a specific way relative to the transducer orifice. All tests were run for 30 seconds, so that a 4-Hz test contained 120 cycles, whereas a 0.5-Hz test contained 15 cycles. Between trials with no changes in the water level or pad, the pad was secured to the block while the actuator was raised to allow relaxation of the pad and return of any water that had been expelled from the rail seat during the previous trial. This seemed to be an effective method for creating repeatable results.

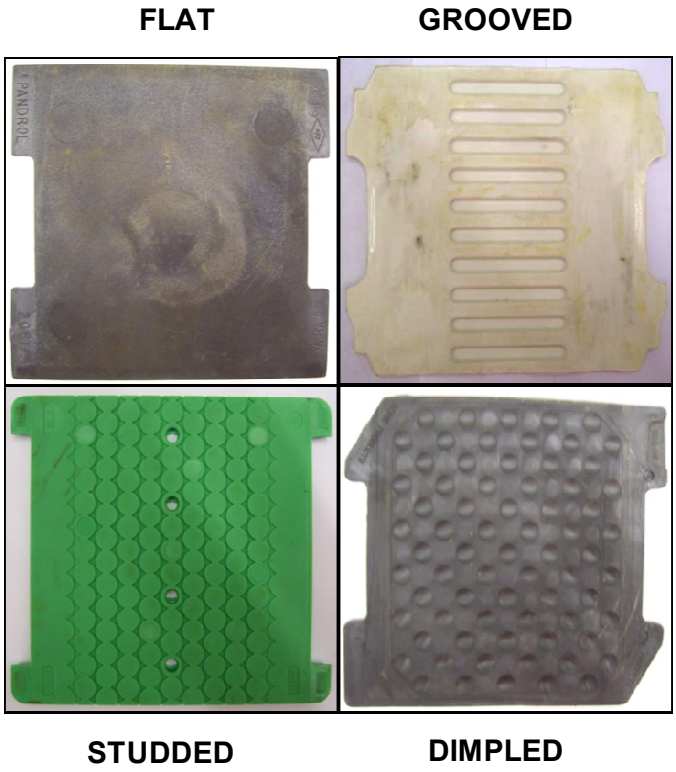

FIGURE 3. TIE PAD SURFACE GEOMETRIES

Results

The data were processed so that the peak pressure values were identified for each trial. The maximum surface pressure p was plotted versus the applied load P to illustrate the correlation between load and surface pressure. By plotting these p-P graphs, it became apparent that the pads exhibited three distinct behaviors related to how much pressure they developed with the same applied load. Figure 4 shows the first group, referred to as "high-pressure pads," and these pads produced pressure close to, though slightly below, the uniform rail seat load stress that Bakharev had assumed. The second group of "low-pressure pads" shown in Figure 5 produced trend lines significantly below, though parallel to, the ideal uniform rail seat stress. The third set of pads was plotted in

Figure 5 with unfilled data points, and this set of pads generated very little pressure, if any, relative to the other pads. See the Appendix for the conversions from US customary units to SI units.

The studded pad, which was the only pad to have narrow channels running along its full length (providing openings at the pad boundaries), did not generate any significant pressure in any of its trials. The same results were observed when a dimpled pad and a grooved pad were modified to provide 2-millimeter-wide channels from the indentation above the transducer to the pads' edges.

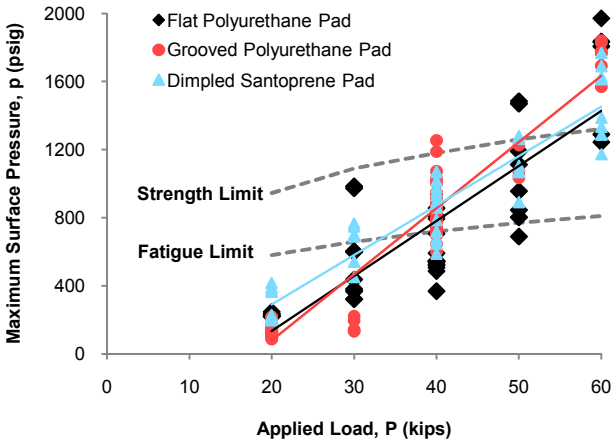

FIGURE 4. COMPARING MAXIMUM SURFACE PRESSURE AND DAMAGE LIMITS, FOR HIGH-PRESSURE PADS

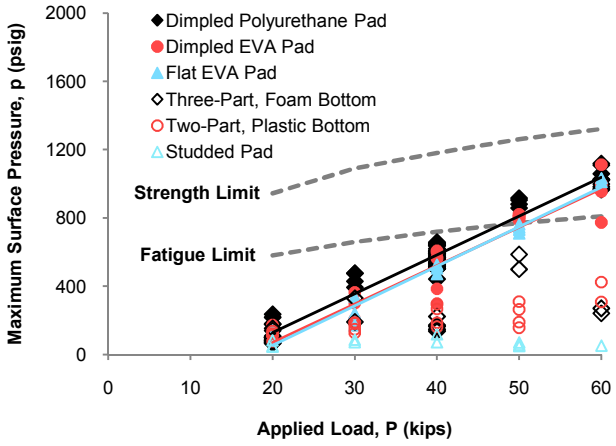

FIGURE 5. COMPARING MAXIMUM SURFACE PRESSURE AND DAMAGE LIMITS, FOR LOW-PRESSURE PADS

The peak pressures *p* were plotted versus the load cycle count *n* to illustrate how the pressure varied during the course of a test. Some *p*-*n* data for a 40-kip (178-kN) applied load are shown for the high-pressure pads in Figure 6 and for the low-pressure pads in Figure 7. Typically, the maximum pressure occurred in the first few cycles of the trial. In some trials, the peak surface pressure was constant with continued load cycles. In other trials, the peak surface pressure dissipated from an initial maximum to either a steady state pressure that it sustained to the end of the test or a negligible value that was nominally zero pressure. The *p*-*n* data shown here for 40 kips (178 kN) is representative of the range of behavior that was observed for other magnitudes of applied load.

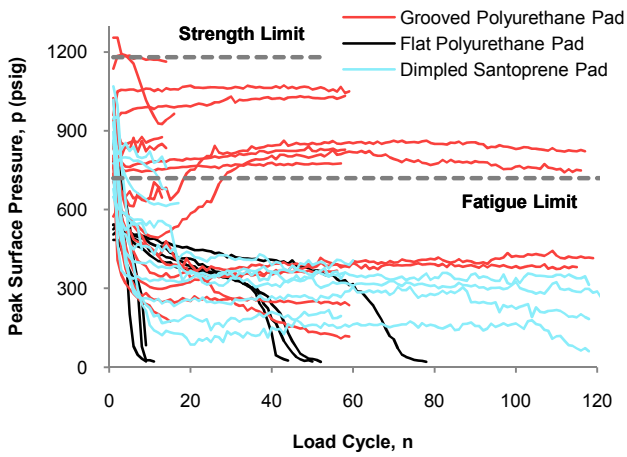

FIGURE 6. RECORDED SURFACE PRESSURE PEAKS FOR HIGH-PRESSURE PADS, 40-KIP APPLIED LOAD

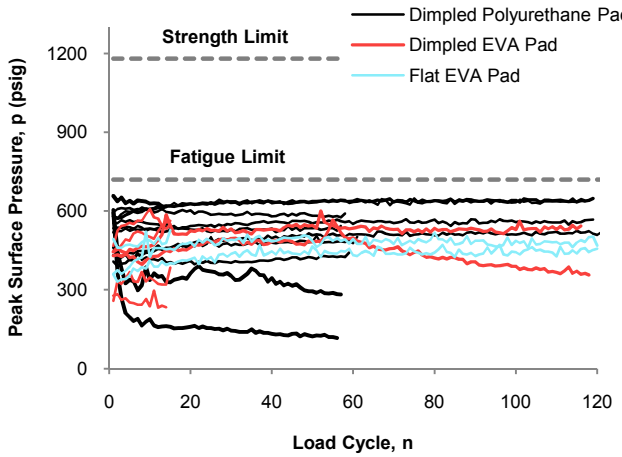

FIGURE 7. RECORDED SURFACE PRESSURE PEAKS FOR LOW-PRESSURE PADS, 40-KIP APPLIED LOAD

While running the tests over the course of many days, it was observed that the actuator's loading plate would shift position relative to the block as a result of the flexibility of the frame. It was observed that if the actuator-to-block interface was mismatched – if there was a nonzero contact angle – this would have a noticeable effect on the *p*-*n* curves and the maximum pressure. As an example, the curves for flat

polyurethane in Figure 6 came from two different test days, with the curves dropping to zero within 10 cycles occurring separately from the curves dropping to zero after 40 cycles. This difference may have been related to changes in the contact angle at the interface.

DISCUSSION

Sources of Variability

Linear trend lines fit the *p-P* data well, with the worst R-squared value at 0.72 for the flat polyurethane pad – the rest of the pads with trend lines had R-squared values at or above 0.88. Trend lines were not fitted to the studded pad or the assemblies because their data were well below the predicted fatigue limit. The *p-P* points plotted in Figures 4 and 5 include data from tests with different water levels, waveforms, and indentation alignments, where applicable. The fact that the data still plots with a good linear fit suggests that such parameters as surrounding water head and loading rate (train speed) do not have a strong influence on the surface pressure. Also, analysis isolating these two variables did not show any significant trends in the resulting surface pressure.

The most likely source of variability in the test results was the difficulty in controlling the relative contact angle between the loading plate and the rail seat block. When advancing the actuator with a relative contact angle between the loading plate and the block, this most likely allows the surface water one direction in which it can escape more easily. On the other hand, if there were a zero relative contact angle, there would be an increased chance that a seal would develop between the pad and the concrete before the surface water could be forced out [2]. This may explain some of the scatter in the maximum pressure generated, as well as the variations in *p-n* behavior, particularly for the flat polyurethane's different pressure loss rates (Figure 6). The potential implications in track are that rail roll or tilt could lead to similar non-zero contact angles between the rail base and the rail seat. So if relative contact angle occurs, it may reduce the rail seat surface pressure that is generated in track.

As for the variable *p-n* behavior of the grooved polyurethane pad (Figure 6), it appears that the trials with the greatest sustained pressure largely occurred when the groove indentation (see Figure 3) was directly above the transducer. The set of trials with the pressure just above the fatigue limit mostly came from the case of the transducer aligned between two indentations, and the set of trials with the greatest pressure loss for the grooved polyurethane pad mostly came from the case of the transducer aligned with the long edge of an indentation. So for the pads with geometry, some of the variability in *p-n* behavior may be explained by changes in indentation alignment.

Surface Water Pressure and Velocity

In Bakharev's model of hydraulic pressure, it was assumed that the surface pressure generated by a load *P* would be equal to *P* divided by the area of the rail seat, which is referred to here as the rail seat load stress. This assumes that the pad and the rail seat are separated by a film of water that transfers the load. For the surface water to ideally transfer load, a seal must be created between the tie pad and the concrete to prevent water from being ejected rather than pressurized. The *p-P* trend lines for the high-pressure pads are close to this ideal rail seat load stress, suggesting that the high-pressure pads match Bakharev's assumption well.

The low-pressure pads exhibited very consistent *p-P* behavior that was parallel to but significantly below the ideal rail seat load stress assumption. One way to explain these results is to consider the transfer of energy through the system. The applied load acts as an energy input that is transferred through the pad to the rail seat block. If water is between the pad and the rail seat, then energy is also transferred to the water. Borrowing from the Bernoulli equation for pipe flow, neglecting changes in elevation [14], we considered the surface water's total energy as the sum of its pressure energy and velocity energy. If a perfect seal is created, and there is no air in the transducer chamber, then all of the load energy would be transferred as pressure energy in the water. Neglecting any dynamic effects and assuming uniform load distribution, it can be assumed that the rail seat load stress is a maximum for the surface pressure that can be generated under a given load – representing the case where the total energy is pressure energy. But if water is allowed to escape or fill air voids, then some of the energy would be manifested as velocity, reducing the pressure that can be generated. So allowing some of the water to escape or flow rather than be pressurized may explain the difference between the high- and low-pressure pads.

This same concept of energy transfer can be applied to offer an explanation for the varied *p-n* results in Figures 6 and 7. There were three general types of *p-n* behavior observed: constant pressure with continued cycles, pressure loss from a maximum to a steady state pressure, and pressure loss from a maximum to effectively zero pressure. What may be causing pressure loss with load cycles is that some volume of water is squeezed out either from within the transducer chamber or from the indentations of the pad. As a pad relaxes between cycles, there would still be at least 5 kips of load applied to the pad, so there may be enough of a seal that water will not return between cycles. Rather, there will be a reduced volume of water in the chamber, requiring the pad to locally flex more into the chamber to pressurize the water. As a result of this loss of contact with the water, the stress distribution on the pad may change so that most of the stress is transferred away from the transducer's orifice. If the volume of water in the transducer chamber gets low enough, the pad may become unable to contact the water and pressurize it, resulting in an apparent zero pressure reading.

Comparison of Tie Pads

The grooved and flat polyurethane pad surfaces were two sides of the same tie pad. These surfaces generated very similar *p-P* curves, but consistently different *p-n* behavior, providing strong evidence that surface geometry can lead to

more sustained pressures with load cycles – the indentations may act as storage compartments for the surface water or they may introduce more tortuous escape paths than a flat surface would. However, the dimpled and flat EVA pads generated similar *p-P* and *p-n* graphs, despite the difference in surface geometry. It is important to note that the dimpled EVA and flat EVA are different pads with different thicknesses, so it is not quite the same comparison as with the grooved and flat polyurethane. Generally EVA is a stiffer material than polyurethane. But this introduces another complication when comparing these tie pads: though the two EVA pads are nominally the same material, there is room for variation of material properties to fit a specific product, similar to how a concrete mix is adjusted to produce different strengths. The same can be said about the dimpled and the flat polyurethane pads – they appear to have slightly different stiffness and hardness properties. The major difference between the dimpled santoprene and the dimpled polyurethane pads is that the santoprene rubber was relatively very flexible and underwent permanent deformation after a few trials. It is suspected that the santoprene pad deforms enough that the dimples are flattened during the trials, causing it to act more like the flat polyurethane pad, in terms of surface pressure, than the dimpled polyurethane pad. The material specifications for each pad were not available for comparison for this paper, but it appears that both the surface geometry and the material properties of the pad determine what surface pressures are generated.

A possible explanation for why the studded pad, as well as the dimpled and grooved pads that were modified with channels, generated zero pressure for all of its tests is that the surface water had at least one direct path to escape under applied load rather than being pressurized. As long as the movement of escaping water over the rail seat is less damaging than the pressure that would otherwise be generated – this is likely the case – then providing escape channels in a thermoplastic material appears to be an effective way to prevent hydraulic pressure cracking in the rail seat.

It was observed that both the hardest material – the plastic bottom of the two-part assembly – and the softest material – the foam bottom of the three-part assembly – generated pressures lower than the low-pressure pads. As shown in Figure 5, these pad assemblies developed pressures that would require very high rail seat loads – probably 80 to 90 kips (356 to 402 kN) or higher – to pass the fatigue limit, assuming that the present data can be extrapolated. For the plastic, it is possible that it was difficult to create a seal with such a hard, stiff material, allowing water to escape rather than being pressurized. It was observed during tests that the soft foam bottom would become permanently deformed after one trial. During the first trial, the foam apparently created an adequate seal and developed pressure not too far below the low-pressure pads, with some pressure loss with load cycles. When a subsequent trial was run with the same pad, the same pressure was not obtained, and even lower pressures were generated with subsequently higher loads. This was observed when going from 50 kips to 60 kips (223 to 267 kN) in Figure 5 (from 30 kips to 40 kips (134 to 178 kN) as well), and it may be that the deformation of the foam prevented it from forming a seal and allowed the water to escape.

Potential for Concrete Damage

The strength and fatigue limits from the effective stress model were superimposed on the *p-P* graphs (Figures 4 and 5) for comparison. The high-pressure pads, on average, exceeded the fatigue limit between 30 and 40 kips (134 to 178 kN) applied load and exceeded the strength limit between 50 and 60 kips (223 to 267 kN) applied load. On the other hand, the low-pressure pads exceeded the fatigue limit with 50 kips (223 kN) applied load but did not exceed the strength limit within 60 kips (267 kN). So for rail seat loads above 50 kips (223 kN) there is the potential that a high-pressure pad could initiate spalling in the concrete. It is also possible that fatigue damage could result for either high- or low-pressure pads if the proper conditions are met.

Fatigue damage would require surface pressure exceeding the fatigue limits to be cycled millions of times, and this would require each cycle to have the correct combination of high rail seat loads and moisture in the concrete and on the rail seat. Considering a 286-kip (130-metric-ton) rail car with 4 axles, approximately 36 million gross tons (MGT) (33 million gross metric tons) would be required for 1 million load cycles.

High rail seat loads could result from high dynamic wheel loads – caused by wheel or rail imperfections or support transitions, such as those found adjacent to bridges and grade crossings – or by poor load distribution among adjacent ties. When 20 kips (89 kN) was taken as the static rail seat load, this assumed that one rail seat supports at most half of a wheel load, with the other half of the load distributed to adjacent ties [15]. If adjacent ties are broken, missing, spaced too far apart, or not providing good bearing for the rail, a rail seat could take up to 100% of the wheel load. Based on data from wheel impact load detectors (WILD), the rail seat load could be as high as 90 kips (402 kN) or greater if one rail seat has to take most of the wheel load [16, 17].

Our effective stress model assumed a saturated concrete in order to model the distribution of pore water pressure from an initial surface water pressure. If the concrete is fully saturated, then all of its pores are filled with water. In an unsaturated concrete, the pore volume not taken up by water is filled with air. Considering pressure distribution, a fully saturated concrete is assumed to transfer pressure immediately, just as water contained in a pressure vessel would. However, if the concrete is not fully saturated, pressurized water will try to relieve its pressure by flowing through the pores to fill the air voids. So in an unsaturated case, the pressure at some depth would be lower than what our ideal model predicts. Another way to think of this is that the same surface pressure will potentially do more damage to a saturated concrete than an unsaturated concrete. The important question to answer then is whether concrete ties in track can be fully saturated, even just locally saturated at the rail seat. If not, then the effective stress model presented here would represent a conservative but potentially invalid prediction for concrete damage limits.

A significant assumption of the current model is that the concrete damage limits are based on 7,000-psi 28-day strength. This is the minimum strength AREMA recommends for concrete ties. The reality is that concrete-tie manufacturers in the US commonly use mixes that produce 28-day strengths well above 7,000 psi, reaching up to 11,000 psi. If the model were modified to incorporate higher concrete strengths, the damage limits would effectively shift up on the *p*-*P* and *p*-*n* graphs, representing an increase in the tie's resistance to hydraulic pressure cracking.

The current effective stress model largely represents a conservative, worst-case scenario for hydraulic pressure cracking resistance. One of the useful features of the model is that it has demonstrated the feasibility of hydraulic pressure contributing to RSD. The model requires further modifications to transition from testing the feasibility of a theory to predicting the likelihood that hydraulic pressure will lead to damage for different scenarios. Such modifications should attempt to account for the distributions of rail seat loads, precipitation or ponding events, and concrete strengths that occur in railroad track. These additions will result in a more applied model, possibly useful as a tie-pad design aid.

CONCLUSION

Based on the results of the laboratory experiments and the damage limits defined by our effective stress model, hydraulic pressure cracking appears to have the potential to initiate or contribute to RSD as a concrete deterioration mechanism. It appears that the most effective way to prevent hydraulic pressure is to use pads or pad assembly bottoms that do not seal water. The soft foam and the hard plastic bottoms developed little surface pressure at the rail seat, with the hard plastic being slightly more effective. When thermoplastic pads are in contact with the concrete rail seat, it appears that designing the pad with direct escape channels for the water effectively ejects the surface water upon load application rather than pressurizing it. Thermoplastic pads without escape channels created the highest surface pressures, apparently sealing the water during load application. It seems advisable and relatively simple to incorporate these considerations into future pad and pad assembly designs – balanced with other considerations, such as abrasion durability.

Low rail seat loads, resulting from near-static wheel loads and good load distribution among adjacent ties, will not generate damaging hydraulic pressure at the rail seat, according to our effective stress model. Sufficient moisture for saturated conditions is required for hydraulic pressure to damage the concrete. The continuation of this research will involve combining damage limits that account for variable concrete strength, measured surface pressures for different pads, wheel impact load detector (WILD) data, and what is known about the potential for saturated concrete ties in track to create a more informed prediction about the risk for fatigue damage from hydraulic pressure.

ACKNOWLEDGMENTS

This research was funded by the AAR Technology Scanning Program. The authors would like to thank David Davis and Richard Reiff of TTCI; Ernie Barenberg, Grzegorz Banas, and Tim Prunkard of the University of Illinois at Urbana-Champaign (UIUC); Bill Riehl of RailAmerica Inc.; Dwain Jackson of Transducers Direct; the AAR Technology Scanning Committee; and the members of AREMA Committee 30 – Ties, Subcommittee 4 – Concrete Tie Technology for their invaluable contributions to this research. The authors would also like to acknowledge Mauricio Gutierrez-Romero, Mark Dingler, Kevin Kilroy, Hammad Khalil, Charles Gross, Samantha Chadwick, David Marks, and Joseph Rudd from UIUC and Edgardo Santana-Santiago of the University of Puerto Rico at Mayaguez for their work on this project. John C. Zeman has been supported in part by a CN Research Fellowship in Railroad Engineering. J. Riley Edwards has been supported in part by grants to the UIUC Railroad Engineering Program from CN, CSX, Hanson Professional Services, Norfolk Southern, and the George Krambles Transportation Scholarship Fund.

NOMENCLATURE

A	Cross-sectional area of the tie
b_r	Base width of the rail
b_t	Base width of the tie
c	Distance from neutral axis of section to extreme fiber, assumed to be half the section height
E	Young's modulus of the tie
E_f	Effective resilient modulus of the foundation
E_i	Resilient modulus of layer i
e	Eccentricity of the prestress force
f_t'	Tensile strength of concrete
h_i	Thickness of layer i
I	In-plane moment of inertia of the tie
k	Modulus of the foundation reaction
L	Length of the tie
(L/V)	Ratio of lateral component to vertical component of wheel load
M	In-plane bending moment in the tie
N	Axial prestress force in the tie
n	Load cycle count
P	Component of wheel load supported by the tie, normal to the rail seat surface
p	Surface water pressure at the rail seat
$\mathbf{S}$	Principal state of total stress, a 3x3 diagonal matrix containing the principal stresses
$\mathbf{S'}$	State of effective stress, a 3x3 diagonal matrix in principal coordinates
$\mathbf{S_B}$	Contributions from a prestressed beam on an elastic foundation to the total stress-state, a 3x3 matrix in *xyz* coordinates
$\mathbf{S_H}$	Contributions from a uniform horizontal load to the total stress-state, a 3x3 matrix in *xyz* coordinates
$\mathbf{S_V}$	Contributions from a uniform vertical load to the total stress-state, a 3x3 matrix in *xyz* coordinates

$\mathbf{S}_{xyz}$ State of total stress, a 3x3 matrix in *xyz* coordinates
$\mathbf{U}$ State of stress expression for pore water pressure, a 3x3 diagonal matrix
u Pore water pressure in the concrete
V Shear force in the tie
x Direction along the axis of the rail
y Lateral direction, along the axis of the tie
z Vertical direction, positive downward
v_f Poisson's ratio of the foundation
v_t Poisson's ratio of the tie
σ_i Normal stress on a face perpendicular to the *i*-direction, positive when compressive
τ_{ij} Shear stress on a face perpendicular to the *i*-direction, positive when acting in the *j*-direction

REFERENCES

[1] Zeman, J.C., J.R. Edwards, D.A. Lange, C.P.L. Barkan, "Investigating the Role of Moisture in Concrete Tie Rail Seat Deterioration," *AREMA Conference Proceedings 2009*, American Railway Engineering and Maintenance-of-way Association (AREMA), Landover, Maryland, September 2009.

[2] Zeman, J.C., J.R. Edwards, D.A. Lange, C.P.L. Barkan, "Investigation of Potential Concrete Tie Rail Seat Deterioration Mechanisms: Cavitation Erosion and Hydraulic Pressure Cracking," *Proceedings of the Transportation Research Board 89th Annual Meeting*, Washington, DC, January 2010.

[3] Zeman, J.C., J.R. Edwards, D.A. Lange, C.P.L. Barkan, "Failure Mode and Effect Analysis of Concrete Ties in North America," *Proc. of the 9th International Heavy Haul Conference*, Shanghai, China, June 2009.

[4] Bakharev, T., Chapters 1, 2, 3, 5, 6, and 7, *Microstructural Features of Railseat Deterioration in Concrete Railroad Ties*, M.S. Thesis, University of Illinois at Urbana-Champaign, Urbana, Illinois, 1994, pp. 1-28 and 68-97.

[5] Choros, J., B. Marquis, M. Coltman, "Prevention of Derailments due to Concrete Tie Rail Seat Deterioration," *Proceedings of the ASME/IEEE Joint Rail Conference and the ASME Internal Combustion Engine Division, Spring Technical Conference 2007*, pp. 173-181.

[6] Hjelmstad, K.D., *Fundamentals of Structural Mechanics*, 2nd ed., Springer Science + Business Media, LLC, New York City, New York, 2005, ch. 3 and 7, pp. 103-124 and 241-282.

[7] Poulos, H.G. and E.H. Davis, *Elastic Solutions for Soil and Rock Mechanics*, John Wiley and Sons, New York City, New York, 1974, ch. 1, 3 and 6, pp. 1-2, 54, 66, and 162-164.

[8] Mindess, S., J.F. Young, D. Darwin, *Concrete*, 2nd ed., Pearson Education Inc., Upper Saddle River, New Jersey, 2003, ch. 4 and 13, pp. 68-76 and 342-344.

[9] Naaman, A.E., *Prestressed Concrete Analysis and Design Fundamentals*, 2nd ed., Techno Press 3000, Ann Arbor, Michigan, 2004, ch. 4, pp. 193-195.

[10] Selig, E.T. and D. Li, "Track Modulus: Its Meaning and Factors Influencing It," *Transportation Research Record*, v. 1470, 1994, pp. 47-54.

[11] Cai, Z., G.P. Raymond, R.J. Bathurst, "Estimate of Static Track Modulus Using Elastic Foundation Models," *Transportation Research Record*, v. 1470, 1994, pp. 65-72.

[12] Hetenyí, M. *Beams on Elastic Foundation*, University of Michigan Press, Ann Arbor, Michigan, 1946, ch. 1 and 4, pp. 1-9 and 56-58.

[13] Craig, R.R., *Mechanics of Materials*, 2nd ed., John Wiley & Sons, Inc., New York City, New York, 2000, ch. 3, pp. 81-84.

[14] Munson, B.R, D.F. Young, T.H. Okiishi, *Fundamentals of Fluid Mechanics*, 5th ed., John Wiley & Sons, Inc., Hoboken, New Jersey, 2006, ch. 2, 8, and 9 and Appendix B, pp. 39, 402-407, 489-492, 761.

[15] *AREMA Manual for Railway Engineering*, American Railway Engineering and Maintenance-of-Way Association (AREMA), Landover, Maryland, 2009, v 1, ch. 30, parts 2 and 4.

[16] Ameen, P.T., B.J. Pague, "Advanced Technology Safety Initiative: Equipment Health Management System," Association of American Railroads, Circular Letter (c-9907), August 26, 2004.

[17] Gemeiner, B., S. Mattson, "Wheel Impact Loads and Transmission into Track Structure," *Transportation Research Board 84th Annual Meeting*, AR060 Committee for Railway Maintenance, Washington, DC, January 2005.

APPENDIX

TABLE 1. CONVERSIONS FROM US CUSTOMARY UNITS TO SI UNITS, FOR THE FIGURES

Depth		Pressure		Load	
in	*cm*	*psi*	*MPa*	*kips*	*kN*
1	2.5	300	2.1	10	45
2	5.1	400	2.8	20	89
3	7.6	500	3.4	30	134
4	10.2	600	4.1	40	178
5	12.7	800	5.5	50	223
		900	6.2	60	267
		1000	6.9		
		1200	8.3		
		1500	10.3		
		1600	11.0		
		2000	13.8		